

# We are IntechOpen, the world's leading publisher of Open Access books Built by scientists, for scientists

6,300

Open access books available

170,000

International authors and editors

185M

Downloads

Our authors are among the

154

Countries delivered to

TOP 1%

most cited scientists

12.2%

Contributors from top 500 universities



WEB OF SCIENCE™

Selection of our books indexed in the Book Citation Index  
in Web of Science™ Core Collection (BKCI)

Interested in publishing with us?  
Contact [book.department@intechopen.com](mailto:book.department@intechopen.com)

Numbers displayed above are based on latest data collected.  
For more information visit [www.intechopen.com](http://www.intechopen.com)



Chapter

# Additively Manufactured High-Strength Aluminum Alloys: A Review

*Fahad Zafar, Ana Reis, Manuel Vieira and Omid Emadina*

## Abstract

This chapter summarizes the recent advances in additive manufacturing of high-strength aluminum alloys, the challenges of printability, and defects in their builds. It further intends to provide an overview of the state of the art by outlining potential strategies for the fabrication of bulk products using these alloys without cracking. These strategies include identifying a suitable processing window of additive manufacturing using metallic powders of conventional high-strength aluminum alloys, pre-alloying the powders, and developing advanced aluminum-based composites with reinforcements introduced either by *in situ* or *ex situ* methods. The resulting microstructures and the relationship between these alloys' microstructure and mechanical properties have been discussed. Since post-processing is inevitable in several critical applications, the chapter concludes with a brief account of post-manufacturing heat treatment processes of additively manufactured aluminum alloys.

**Keywords:** additive manufacturing, high strength, aluminum alloy, advanced processing, challenges, defects, advanced composites

## 1. Introduction

Additive manufacturing (AM) of aluminum (Al) alloys has found industrial applications and now has become a firmly established field. The number of research publications regarding Laser Powder Bed Fusion (L-PBF), one of the most popular AM processes, has shown an exponential increase during the last decade [1]. This trend is certainly not unpredictable, considering the prior wide industrial use of conventional Al-alloys due to their lightweight, high specific strength, and corrosion resistance. AM further broadens the horizon of applications for Al-alloys by its ability to produce complex geometric shapes with hollow sections for weight reductions [2]. The high-strength aluminum alloys (HSAAs) are particularly interesting in the aerospace and automotive industries. Special efforts have been directed at AM of HSAAs, and interesting advances have been made in this field [3, 4], especially in the last decade. Since the L-PBF technique has attracted the most research interest and shown promising results with HSAAs, most of the discussion and references made in this chapter will be focused on L-PBF of HSAAs, limitations in processing, strengthening

mechanisms, recent achievements, defects in printed materials, and possible strategies to overcome them.

Directed energy deposition (DED) [5] and wire arc additive manufacturing [6] processes have also been utilized for the manufacturing of HSAAAs. Since DED offers freedom from restriction to use a closed chamber and offers the possibility of printing large structures, a brief review of DED of HSAAAs is presented in this chapter.

## 2. Laser powder bed fusion of aluminum alloys

Most of the foundry alloys, especially those designed for casting with near-eutectic compositions, are readily printable with negligible risk of cracking, sufficient fluidity, and minimal hot tearing susceptibility (HTS). These favorable characteristics have attracted immense research interest and led to accelerated development in AM of Al-Si alloys. But these alloys could only achieve a low-medium yield strength of <300 MPa. In contrast, some wrought alloys (2xxx, 7xxx series) can achieve far higher (~300–500 MPa) yield strength. However, these alloys have not been found readily printable by L-PBF [7, 8].

### 2.1 Limitations in processing

The L-PBF production of HSAAAs faces challenges such as characteristic columnar microstructure eventually promoting hot cracking susceptibility (HCS) [9, 10], wide solidification range [11], solute loss due to evaporation [12], limited scanning speed to avoid cracking [13], balling, oxidation, and gas porosity.

Columnar grain growth is typically observed in L-PBF processing of Al-alloys due to the direction of the maximum thermal gradient [14]. In addition, for a certain set of L-PBF process parameters, multiple ratios of temperature gradient ( $G$ ) and growth rate ( $R$ ) may exist in the melt pool favoring columnar growth (either in cellular, planar, or dendritic mode). This columnar growth, more specifically the cellular or dendritic growth, leads to poor strain accommodation, and degraded liquid permeability eventually leading to high HCS [15] as shown in **Figure 1a–f**.

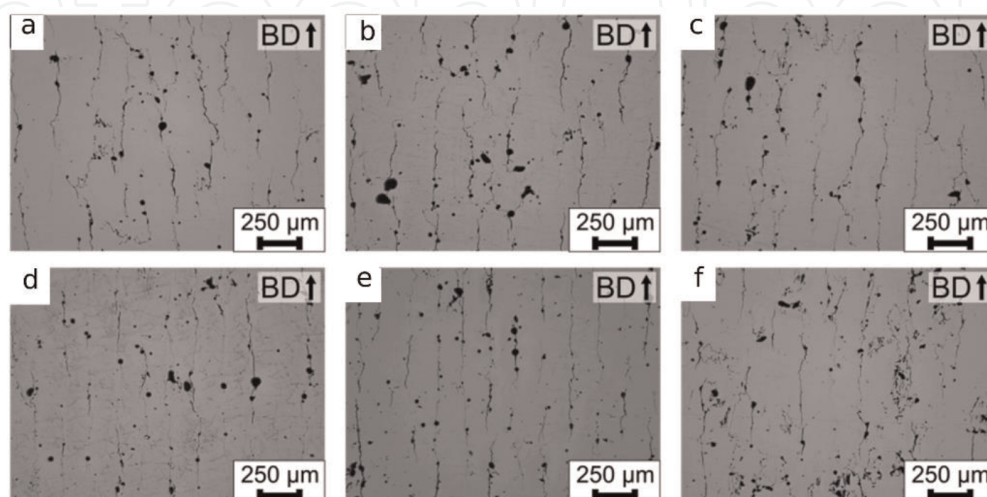


**Figure 1.** (a–f) Solidification cracking observed in AlMg<sub>4.5</sub>Mn<sub>0.7</sub> (re-printed from [16]).

HSAAs tend to have a wide solidification range (or freezing interval), which results in diminished backfill of liquid between coarse columnar crystals [17]. Solute loss occurs due to high processing temperatures during L-PBF, lower boiling points of certain alloying elements and their associated higher equilibrium vapor pressures (than that of aluminum). **Table 1** gives numerical figures for the evaporation of Zn and Mg in three different Al-alloys during L-PBF [12].

In metal deposition during additive manufacturing, liquid metal may not wet the impinging layer (or substrate) due to the surface tension of the liquid. To minimize the surface energy, the deposited liquid metal takes a spherical shape, termed *balling* (see **Figure 2a**).

Alloy	State	Zn%	Mg%	Ni%	Mn%	Cu%	Fe%	Cr%	Si%
AA2017	Before	0.21	0.72	0.009	0.57	4.0	0.40	0.016	0.56
	After	0.07	0.48	0.013	0.61	3.9	0.50	0.035	0.58
AA7020	Before	4.3	1.3	0.006	0.29	0.10	0.29	0.13	0.077
	After	3.0	1.0	0.009	0.30	0.17	0.31	0.14	0.13
AA7075	Before	5.8	2.6	0.007	0.054	1.4	0.25	0.18	0.081
	After	3.9	2.1	0.007	0.057	1.5	0.27	0.20	0.11

**Table 1.**  
 Solute element concentration before and after L-PBF [12].

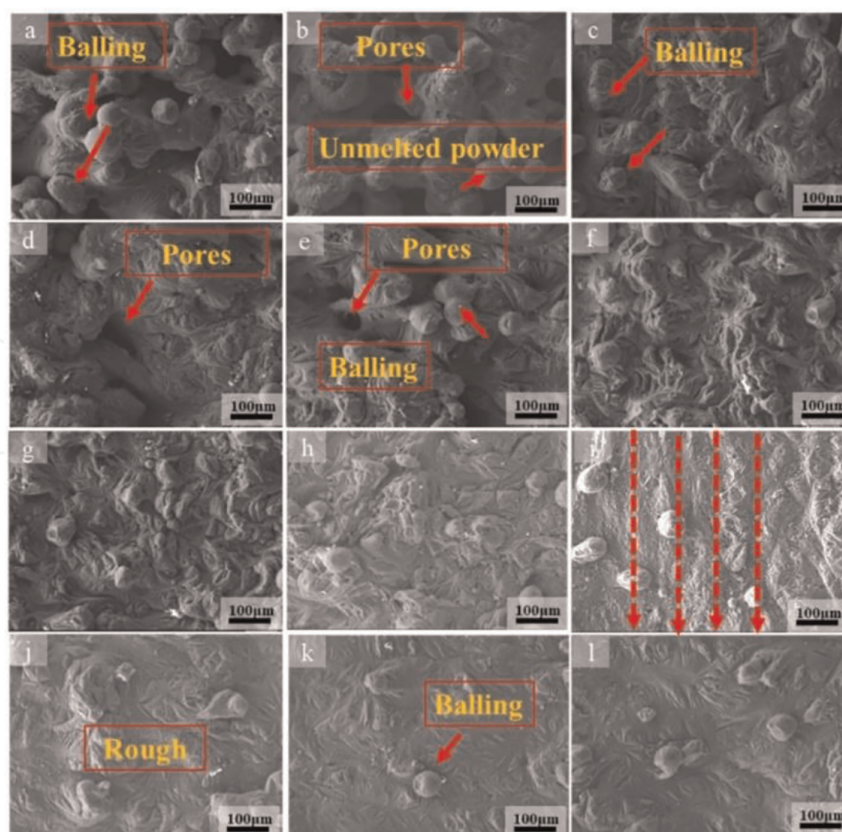


**Figure 2.**  
 (a–i) Micrographs of selective laser-melted AZ61 magnesium alloy under different laser scanning speeds showing balling and porosity defects (re-printed from [18]).

Being highly reactive toward atmospheric oxygen, aluminum alloys tend to oxidize readily by reaction with a small quantity of oxygen trapped in the air gaps between aluminum powders, which causes inferior quality in L-PBF deposited HSAAAs [19].

Porosity defect has been widely reported as well as investigated in Al-alloys, and a porosity of 0.5% is generally termed acceptable in AM Al-alloys [20]. Insufficient melting of powder (or lower than the optimum volume energy density of laser) [21], moisture absorption in Al-powder from the atmosphere [21], spatter and smoke formation during AM process [22], and use of helium as inert gas for the process [23] can increase the porosity of resulting AM product.

## 2.2 Trends in the elimination of defects

Continued efforts have been made in the past decade to overcome the problems discussed above. Broadly, three main strategies have gained particular attention, showing promising results with HSAAAs. These strategies are briefly listed below, and a discussion of their application and limitations will follow:

1. *Designing of new alloys*, to provide further strengthening, primarily by solid solution strengthening and/or grain boundary strengthening. Transition elements and/or rare-earth elements (e.g., Sc and Zr) have gained particular interest in this regard as dispersoids. Further strengthening through precipitation hardening may also be possible.
2. *Tailoring material or process for adaptation of existing HSAAAs for AM*. This strategy seeks to enable AM of existing high-strength wrought aluminum alloys (e.g., AA2024, AA7075, and AA2219) and adapt them to AM by modifying them to diminish solidification cracking (most frequent limitation for AM of these alloys). Tailoring process parameters and defining the process window to print such existing wrought HSAAAs have proved less successful. Existing high-strength foundry-grade Al-alloys can also be additively manufactured similarly.
3. *Development of advanced composite materials for AM*. This approach involves the distribution of fine (micro/nano-sized) ceramic/carbon-based reinforcement or facilitating *in situ* reaction to generate a reinforcing phase to strengthen Al-alloys.

Though designers prefer to utilize existing materials with sufficient reliable property data, it should be kept in mind that even well-established alloys present a significantly different microstructure after additive manufacturing due to rapid thermal processing. While in the previous discussion, three different strategies are presented for the elimination of defects in HSAAAs, there is some overlap in these strategies to achieve an acceptable set of properties in the AM HSAAAs. Moreover, there are several interdependent factors that affect the printability and the quality of the final AM product, which cannot all be discussed at length here, provided the scope of this text. **Figure 3** presents these factors, stemming either from the raw materials or the AM processing strategy.

## 2.3 Grain refinement strategy

The addition of nucleating agents to achieve the heterogeneous nucleation of aluminum grains upon the potent primary particles is utilized for grain refinement in



**Figure 3.**  
*Factors influencing the properties in additively manufactured HSAAs.*

HSAAs. The heterogeneous nucleation promotes the formation of equiaxed grains. Such grain refinement leading to equiaxed grains is highly desirable as it offers benefits, such as reduced susceptibility to hot tearing, higher strength, lesser anisotropy, and shrinkage porosity.

A consequent reduction in the fraction of columnar grains enhances the printability of HSAAs. For equiaxed growth of a crystal, heat must dissipate from the crystal to melt ( $G < 0$ ) [24]. In contrast, during L-PBF, heat dissipates from the melt to crystals and onward down to the substrate ( $G > 0$ ). Thus, high enough undercooling is required to promote equiaxed grain growth. The heterogeneous nucleation diminishes the nucleation barrier by facilitating the growth of Al matrix crystals on preexisting nuclei that have a small lattice parameter misfit with that of the matrix [25]. As the growth of equiaxed grains progresses on nuclei, they impinge upon the neighboring equiaxed grains as well as the growing columnar grains, which restrict columnar growth. This phenomenon is termed as “columnar to equiaxed transition” (CET) in the solidification processing literature. The reduction in columnar grain growth also reduces the crack susceptibility in the AM HSAAs, which is a common problem faced during L-PBF of conventional wrought aluminum alloy grades.

The transition metal Scandium (Sc) and Zirconium (Zr) have best served this purpose [26, 27]. Sc provides exceptional grain refinement in aluminum alloys. The primary Sc-containing particles serve as heterogeneous nuclei, which can mitigate solidification cracking. Sc alloying imparts a significant precipitation hardening in aluminum alloys, though it is limited by the solid solubility of Sc (0.4%) in aluminum. However, rapid solidification rates in the L-PBF process enable the retention of as

much as double this quantity in solution, which can be precipitation strengthened by nano- $\text{Al}_3\text{Sc}$  precipitates during subsequent ageing treatment at 250–300°C [28]. Sc also restricts grain growth in aluminum alloys since  $\text{Al}_3\text{Sc}$  dispersoids serve to pin the grain boundaries and stabilize the grain structure [29]. These  $\text{Al}_3\text{Sc}$  particles have a small mismatch of lattice parameter with that of the aluminum matrix (0.4103 nm vs 0.4049 nm), which makes them highly effective nucleation sites for  $\alpha$ -aluminum grains. In aluminum alloys, every 0.1% wt. Sc provides a 40–50 MPa increment in yield strength. This increase results from the precipitation strengthening by the formation of  $\text{L}_{12}$  coherent precipitates ( $\text{Al}_3\text{Sc}$ ) during aging heat treatment [30]. Upon further addition of transition metals with low diffusivity in aluminum, such as Ti, Zr, and Hf can partially substitute Sc atoms forming precipitates such as  $\text{Al}_3\text{Sc}_{1-x}\text{Zr}_x$ . These resulting precipitates are highly resistant to further coarsening due to core-shell-like structure, and they offer a further advantage of high-temperature stability (aged at 325°C) [31] as compared with precipitates of conventional precipitation-hardened aluminum alloys (typically aged  $\sim$ 120–190°C). However, Sc has been identified as a critical raw material by European Commission [32], and alternates must be explored to offer a competitive advantage.

In an Al-Zn-Mg-Cu-Ta alloy, Ta forms *in situ* primary  $\text{Al}_3\text{Ta}$  particles and can dissolve in the second phase  $\text{Al}_2\text{Cu}$  to restrict further coarsening during heating cycles [33].

**Figure 4** presents the tensile yield strengths achieved in state-of-the-art HSAA bearing Sc and Zr, which clearly shows a possibility to achieve a yield strength higher than 500 MPa with an acceptable ductility.

Though it is worth mentioning here that multiple strengthening mechanisms may play role in strengthening, with the dominance of one or the other mechanism in the case of a particular HSAA (for further insight into strengthening mechanisms, see Ref. [34]).

## 2.4 Eutectic strategy and narrowing down the freezing range

Eutectic strategy is more commonly applied in L-PBF of Al-Si alloys, which facilitates sufficient backfilling of cracks. The terminal stage of solidification [35] is

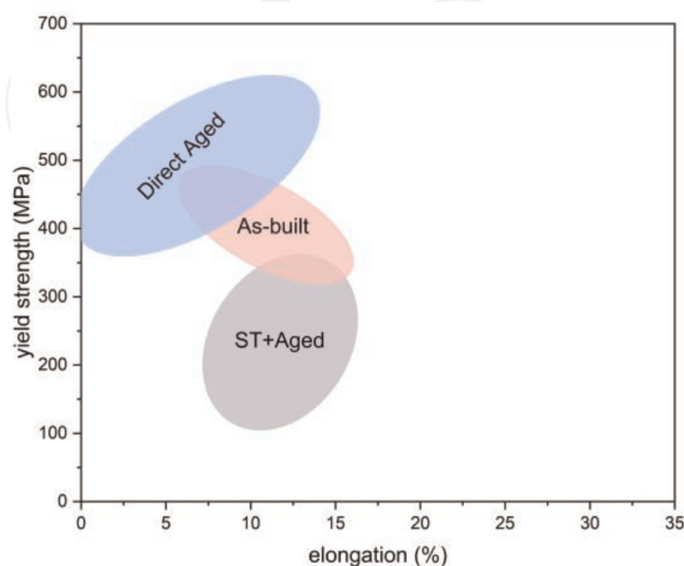


**Figure 4.** Tensile yield strength (95% confidence mean) of recent Zr, Sc-strengthened HSAA.

considered a stage with the highest hot cracking susceptibility. The conventional wrought high strength age-hardenable alloys (2xxx, 7xxx) contain alloying elements, which tend to widen their solidification range, leading to the segregation of low melting point phases during grain growth [36]. The solidification range is defined as the difference between the liquidus and solidus temperatures of the alloy. Inspired by the excellent printability of Al-Si alloys, researchers were tempted to use Si as an additive to the metal powder of existing wrought aluminum alloys. Pre-alloying with 3.74 wt.% Si reduced the freezing interval and eventually decreased the solidification cracking susceptibility in modified Al-7075 [37]. In another study, ultimate tensile strength and yield strength of 548 and 403 MPa were achieved in a newly designed alloy with Si alloying wherein numerous Al-Mg<sub>2</sub>Si fine eutectics were formed in situ upon L-PBF, which helped mitigate solidification cracking [38]. The addition of Ce in the Al matrix narrows down the freezing range. Al-3Ce-7Cu was printed successfully with 0.03% porosity and a UTS of 456 MPa in as printed condition. The alloy showed good tensile strength (UTS:186 MPa, YS:176MPa) at 250°C as well [39].

## 2.5 Post-processing heat treatment

High cooling rates inherent to AM process enable the achievement of unique metastable microstructures in the as-fabricated parts, which are readily transformed to equilibrium phases upon exposure to high temperatures. It is a common practice in industries to carry out a stress-relieving heat treatment to diminish the risk of distortion or cracking due to high residual stresses after rapid thermal cycling of AM processes like L-PBF. Although in most cases, a simple heat treatment cycle serves for the intended application of AM products, some demanding applications may require a combination of this heat treatment with hot isostatic pressing.

As a general observation in the case of AM aluminum alloys, the conventional heat treatment procedures applicable for cast/wrought aluminum alloys involving solution heat treatment and ageing destroy the strengthening benefits gained through L-PBF, whereas a direct aging treatment can retain some of these benefits and still sufficiently relieves the residual stresses [40].

A typical problem faced by precipitation strengthened (e.g., Al 2xxx) aluminum alloys is posed by their low ageing temperature. While these alloys are age-hardened for strengthening between 150 and 200°C, this temperature is not high enough to relieve the residual stresses in the L-PBF parts, which need a temperature around 300°C. If stress relief is carried out at 300°C, strength in these alloys may only be regained by solution treatment followed by precipitation hardening. However, solution treatment of L-PBF precipitation hardenable alloys eradicates the beneficial effects of rapid solidification gained by rapid laser processing. Hence, it is difficult to use typical heat-treatable aluminum alloy for laser processing and gain its advantage originally inherent to artificially aged wrought aluminum alloys.

Alternatively, an alloy that can be age-hardened (or retain the strength gained during AM) at a stress-relieving temperature of ~300°C may serve as a HSAA. Such an alloy can retain the gained strength while still relieving the residual stresses with a single aging treatment (direct aging). The addition of a slow diffusion element (like Sc/Zr) to conventionally non-heat treatable Al-alloys of 3xxx and 5xxx series has induced remarkable strengthening since they tend to age-harden at much higher temperatures ( $\geq 300^\circ\text{C}$ ) (see **Table 2**).

**Figure 5** presents the alloying element(s)-wise tensile yield strength (YS) and elongation% of some selected HSAA's from the research literature. It can be observed



Alloy	Year	Post-process	UTS (MPa)	YS (MPa)	el. %	P, SS, t, HS*	Ref.
Al-Mg-Sc-Zr	2020	St + aged	511	504	7.3	325, 1200, 30, 80	[41]
Al-Mn-Mg(Sc/Hf/Zr modified)	2022	As built	504	438	10.9	300, 700, 30, 105	[42]
Al-Mn-Mg(Sc/Hf/Zr modified)	2022	D-Ageing	542	487	7.4	300, 700, 30, 105	[42]
Al-Mn-Sc	2022	As built	412	395	21	350, 1600, 30, 100	[43]
Al-Mn-Sc	2022	D-Ageing	572	559	9.8	350, 1600, 30, 100	[43]
Al-Mn-Sc	2020	D-Ageing	573	571	16	370, 1000, 30, 100	[44]
Al-Mn-Mg-Sc-Zr	2021	As built	703	508	8.2	190, 700, 30, 100	[45]
Al-Mn-Mg-Sc-Zr	2021	D-Ageing	712	621	4.5	190, 700, 30, 100	[45]
Al-Mg-Si-Sc-Zr	2021	St + aged	580	385	19	160, 200, x, x	[46]

\*P—power (watts), SS—scan speed (mm/s), t—layer thickness (mm), HS—hatch spacing (μm).  
 D-Ageing—Direct aging, St + aged—solution treated and artificially aged.

**Table 2.**  
 Mechanical properties and process parameters of Sc, Zr alloyed HSAAAs.

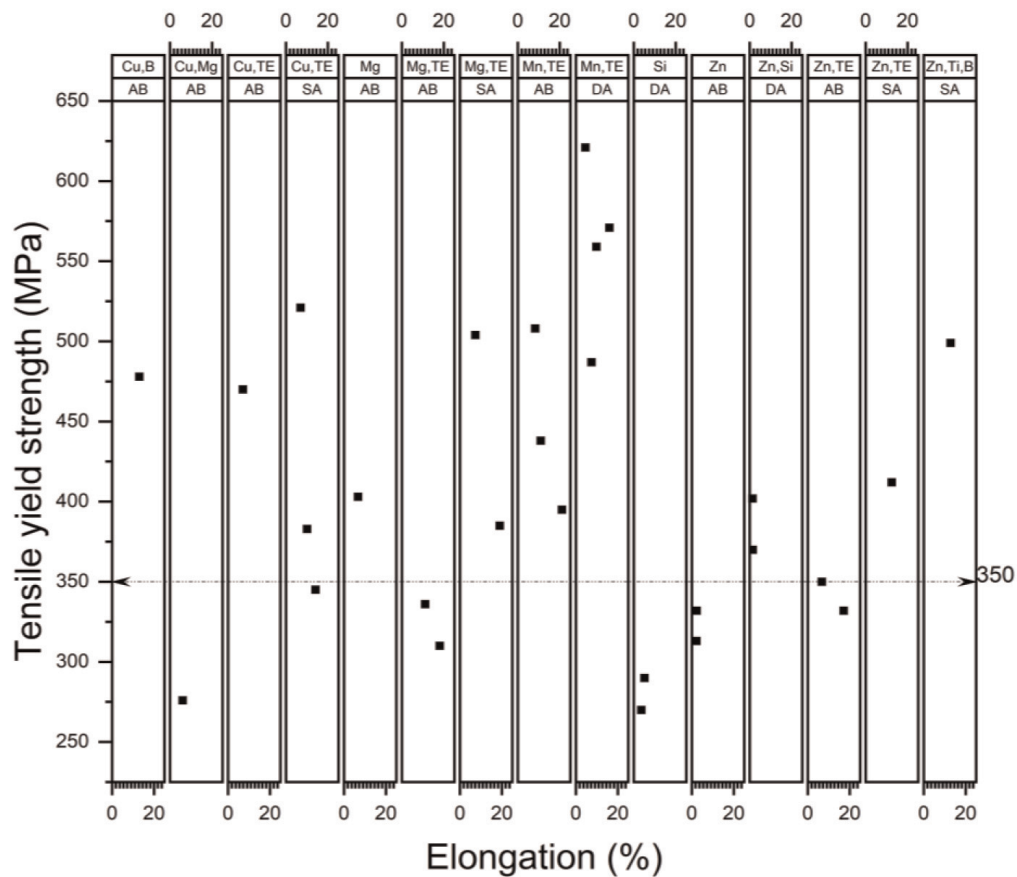


**Figure 5.**  
 Alloying element-wise tensile yield strength and elongation of selected high-strength alloys [11, 14, 38, 41–57].  
 TE—transition element(s), AB—as-built, SA—solution treated and aged, DA—Direct aging.

that many of these alloys demonstrate a YS higher than 350 MPa (comparable with that of conventional wrought HSAAs).

It can be inferred from **Figure 5** that a yield strength superior to 550 MPa and reasonable ductility can be achieved in Al-Mn-transition element(s) alloy after direct aging heat treatment. Without alloying of transition elements, a yield strength superior to 450 MPa has been achieved with close to 10% elongation in L-PBF using Al-Zn + Ti, B and Al-Cu + CaB<sub>6</sub> (composite ball-milled powders).

### **3. Directed energy deposition of aluminum alloys**

Directed energy deposition (DED) is defined as a process in which focused thermal (laser, electron, or plasma) energy melts the feedstock material during deposition. Argon or nitrogen gas is used as a shielding gas to protect against the formation of aluminum oxide scale during thermal exposure. The most widely applied DED processes are wire arc additive manufacturing (WAAM) and laser DED (or Laser-engineered net shaping) processes.

Several studies investigated the deposition of aluminum alloys by laser-directed energy deposition (DED) [58, 59]. However, the results are not much promising, and several challenges lie ahead of DED of aluminum alloys to compete with conventional wrought alloys or their additively manufactured L-PBF counterparts.

DED of high-strength aluminum alloys faces technical challenges due to the high surface reflectivity of Aluminum, and higher laser power input is required to melt the blown aluminum powder completely [60]. This in turn leads to gas porosity by selective evaporation of lighter constituent elements such as Magnesium and Zinc [58, 61]. The high coefficient of thermal expansion (CTE) of aluminum alloys leads to shrinkage upon solidification followed by cracking or severe deformation due to intense repetitive thermal cycling during the DED process [62]. The inherent tendency of surface oxidation and moisture absorption from the atmosphere [62, 63] and poor flowability of powder, owing to low density, adversely affects the powder mass flow rate, which results in inferior quality of deposit [64].

In more recent studies on DED of high-strength Al-7075 alloy using gas-atomized powders, a crack-free, low-defect bulk material was deposited having an ultimate tensile strength of  $222 \pm 17$  MPa and an elongation of 2%, which is significantly lower than the wrought 7075-T6 [65]. Moreover, the hardness only increased from  $(85 \pm 4)$  HV0.5 to  $(93 \pm 2)$  HV0.5 upon artificial aging. In another study on DED of Al-7050 alloy, hardness of a 100HV was achieved in an as-built, defect-free bulk deposit; subsequent heat treatment increased the hardness to 128 HV [61]. Due to the relative ease of deposition and wide processing window Al-Si alloys have results comparable with those of cast counterparts; however, as of now, high-strength aluminum alloys could not be deposited successfully with DED.

### **4. Particulate-reinforced aluminum-based composites**

Aluminum matrix composites (AMCs) have already found wide applications in the aerospace and automotive industries. AM of AMCs gained particular interest due to freedom of design possibilities and further opportunities for weight reduction through modification of properties by reinforcement of Al-matrix. Either an *ex situ* or *in situ* approach is utilized for the optimization of microstructure and the resulting

properties in AM. In “*ex situ*” AMCs, the reinforcements are synthesized externally and then added to the matrix, while the reinforcements are synthesized during AM process in the “*in situ*” AMCs. While *ex situ* AMCs synthesized using L-PBF have shown promising results, the limitations such as poor wettability of reinforcement by the Al-matrix, limited ability of grain refinement, and a higher likelihood of residual stress due to difference in thermophysical properties between the reinforcement and the matrix cannot be overruled [66].

Various methods are adopted for mixing powders of metallic alloys (matrix) and reinforcements. The selected method affects the resultant powder morphology and influences the laser reflectivity and the heat transfer process during L-PBF. A list of the selected methods and the factors to consider before choosing a particular process over the others is presented in **Table 3**.

Though the direct mixing process is simple, agglomeration of fine particles (nano-sized) and poor wettability are inevitable.

Ball milling is much popular due to its low cost and wide applicability to several powders. Being a nonequilibrium process, it includes a repetitive sequence of deformation, fracture, and cold welding of metal powder particles [67]. Initially, fracture occurs in brittle reinforcement particles, while cold welding dominates in the Al-matrix powder due to plastic deformation. During this deformation and cold welding, reinforcement powders are dispersed in the matrix. Since the Al-matrix gets harder following deformation and cold welding, once again fracture phase dominates until certain dynamics between cold welding and fracture ensures a stable powder size

Method	Factor	Desirability	Factor Rating
Direct mixing	cost	least	√
	applicability	Max.	√ √ √ √
	use with various vol. fractions	Max.	√ √ √ √
Ball milling	cost	Least	√ √
	applicability	Max.	√ √ √ √
	dispersion in matrix	Max.	√ √ √ √
	time	Least	√ √ √
	flowability	Max.	√
Direct mixing or ball milling + in situ reaction	cost	Least	√ √
	dispersion in matrix	Max.	√ √ √ √
	complexity	Least	√ √ √ √
In situ pre-alloying + gas-atomization	cost	Least	√ √ √ √
	flowability	Max.	√ √ √ √
	dispersion in matrix	Max.	√ √ √ √
	applicability	Max.	√ √ √ √
	complexity	Least	√ √ √ √

**Table 3.**  
Methods for preparation of feedstock for L-PBF.

without agglomeration [68]. Ball milling induces grain refinement in the milled powders, mainly due to high energy input accompanied by severe plastic deformation into the powders. The process includes the generation of various crystal defects (dislocations, point defects), which increase the internal energy of the system (lattice) with the subsequent evolution of final grain boundaries, thus relieving the high energy. Ball milling also offers the freedom of choosing a wide size range of powders/granules as the starting material size. However, the irregular shape, rough surface, and flattening of Al-powder adversely affect the flowability of ball-milled Al-powders. Being highly ductile, Al alloys need longer duration milling cycles as compared with steels or titanium alloys. Han et al. [69] milled 4 vol.% Al<sub>2</sub>O<sub>3</sub>/Al powders with up to 20 h milling using different milling strategies (presented in **Table 4**).

Hence, a careful selection of a processing route for composite feedstock synthesis/production and selection of optimum processing parameters is pivotal to achieve desirable properties in AM of HSAAs.

The laser absorptivity of Al-composite powders tends to increase with the addition of reinforcements, and it increases with an increase in the amount of reinforcement in the composite. For example, the laser absorptivity of AlSi10Mg is 0.09 [70], while TiB<sub>2</sub>/AlSi10Mg composite powder has an absorptivity of 0.71 [71]. Thermal conductivity is another important thermophysical property to consider in the case of Al-matrix composites. Independent of their thermal conductivity, nano-sized reinforcement particles tend to decrease the effective thermal conductivity of the composite powders because they introduce interfacial thermal resistance and scatter the energy carriers [72].

In short, there are several considerations for the selection of an appropriate reinforcement, which are interdependent, and hence, the selection of reinforcement needs due attention. Any change in the physical and thermal property of feedstock can lead to redistribution of the thermal field and causes changes in fluid dynamics.

In a recent study, Al-2024, an age-hardenable Al-alloy powder, was modified by mechanical alloying using the ball milling technique. 0.5 w% of CaB<sub>6</sub> nanoparticles of 200nm (avg. size) were milled with Al-2024 powder (~63 μm) for 2h at 150 rpm, baked for moisture removal, and then printed using the L-PBF technique. A good combination of mechanical properties (UTS: 478 MPa, YS: 428 MPa, el.: 13%),

Process	Step	Powder condition
Milling for 20 h	After 4 h milling	Irregular shape, size > 100 μm
	After 8 h milling	Morphology changed, Size reduced
	After 16 h milling	Fracture took over, Size (several particles) ~20 μm, large particles observed
	After 20 h milling	Fracture continued Size range of smaller particles narrowed further (~20 μm), large particles from previous observation did not fracture
Milling for 20 h, with cyclic 10 min milling and 5 min break		some large and plate-like particles formed
Milling for 20 h, with cyclic 10 min milling and 15 min break		Fewer large particles formed a relatively more quantity of finer powder (<90 μm)

**Table 4.** Ball milling parameter of 4 vol.% Al<sub>2</sub>O<sub>3</sub>/Al [69].

Alloy/ reinforcement (wt. %)	mfg. method/ temper	UTS, YS, el.%	Comp. powder preparation	Laser deposition conditions	Source
		MPa, MPa, %	Method	P, SS, LT, HS, Spot S.*	
Al-Cu-Mg (Al2024)/TiC (2)	L-PBF/as-built	388, 332, 10.2	BM, BPR:5:1, 130 rpm, total milling: 3 h	200, 200, x, 40, 90	[74]
Al-Cu-Mg (Al2024)/TiC (2)	L-PBF/St + aged	507, 456, 6.6	BM, BPR:5:1, 130 rpm, total milling: 3 h	200, 200, x, 40, 90	[74]
Al-Cu-Mg (Al2024)/CaB <sub>6</sub> (1)	L-PBF/as-built	428, 478, 13	BM, BPR:5:1, 150 rpm, total milling: 3 h	200, 1000, x, 30, 100	[50]
AlSi10Mg/TiB <sub>2</sub> + TiC (1.5 + 1.5)	L-PBF/as-built	552, 325, 12	BM, BPR:5:1, 150 rpm, total milling: 4 h	270, 1600, x, 30, 110	[75]
AlSi10Mg/TiC (3)	L-PBF/as-built	453, 267, 4.8	BM, BPR:5:1, 150 rpm, total milling: 4 h	270, 1600, x, 30, 110	[75]
AlSi10Mg/TiB <sub>2</sub> (3)	L-PBF/as-built	361, 200, 3.8	BM, BPR:5:1, 150 rpm, total milling: 4 h	270, 1600, x, 30, 110	[75]
AlSi10Mg/TiB <sub>2</sub> (in- situ synth.)	L-PBF/as-built	501, 320, 12.7	Pre-doped composite powder synthesis	300, x, x, x, x	[76]
Al-Cu-Mg-Ag-Ti-B (pre-doped Al-Cu/ TiB <sub>2</sub> )/TiB <sub>2</sub> (pre- doped) (x)	L-PBF/as-built	403, 317, 10.2	Pre-doped composite powder synthesis		[77]
Al-7075/TiN (x)	WAAM/T6	503.6, x, 10.9	Powders suspended in ethanol gel and pre- placed after each layer deposition	xx	[78]
AlSi10Mg/Nbc (3)	L-PBF/as-built	393, x, 12.7	BM without balls, 71 rpm, total milling: 2 h	300, 500, 150, x, 30	[79]
AlSi10Mg/Nbc (6)	L-PBF/as-built	281, x, 9.8		300, 500, 150, x, 30	[79]

\*P—power (watts) SS—scanning speed (mm/s), LT—layer thickness ( $\mu\text{m}$ ), HS—Hatch spacing ( $\mu\text{m}$ ), Spot S—spot size ( $\mu\text{m}$ ).

**Table 5.**  
Mechanical properties and processing parameters of AMCs.

comparable with those of conventional wrought Al-2024 was achieved in as-built condition. The CaB<sub>6</sub> nanoparticles acted as highly effective heterogeneous nuclei due to low lattice mismatch with Al-matrix and facilitated CET, thus enabling a crack-free build [50].

Extensive research has been conducted to reveal and assess the strengthening mechanisms involved in the strengthening of composites (not discussed in this text), and different strength prediction models have been proposed. A quadratic summation strength prediction model, originally proposed by Clyne and later modified by Sanaty-Zadeh [73], can be used for estimating the strength of nano-composites.

$$\sigma_y = \sigma_{m0} + \sqrt{(\Delta\sigma_{\text{Orowan}})^2 + (\Delta\sigma_{\text{GR}})^2 + (\Delta\sigma_{\text{load}})^2 + (\Delta\sigma_{\text{CTE}})^2 + (\Delta\sigma_{\text{Modulus}})^2} \quad (1)$$

Where  $\sigma_{m0}$  is the yield strength of the unreinforced matrix,  $\Delta\sigma_{Orowan}$  is the contribution by Orowan strengthening,  $\Delta\sigma_{GR}$  is a contribution by grain size strengthening,  $\Delta\sigma_{load}$  is a contribution by load-bearing strengthening,  $\Delta\sigma_{CTE}$  is a contribution by dislocation density strengthening, and  $\Delta\sigma_{Modulus}$  is a contribution by elastic modulus mismatch strengthening.

However, there is no consensus as to which model closely reflects reality, up till now. Since all models assume a perfect distribution of particles and bonding of interfaces, the calculated values from these models are always higher than the experimental values nevertheless showing a similar trend.

**Table 5** presents the powder preparation methods, processing technique(s), mechanical properties, and laser processing conditions used for deposition in the most recent publications. These data also give a fair picture of the most recent HSAA composites and well reflect the possibility of modifying the properties (mechanical strength, wear resistance, etc.) of base aluminum alloy by the addition of appropriate reinforcement. The strengthening in such composites has reportedly been gained through multiple strengthening mechanisms, as mentioned earlier.

## 5. Conclusions

- A high demand exists for readily printable L-PBF high-strength light-weight parts of aluminum alloys and such alloys have been introduced.
- One of the simplest and currently feasible ways to achieve high strength is possible through using pre-alloyed Al alloy powder having Mn, Zr, Sc or Mg, Zr, and Sc, which enables to gain the benefit of high strength and stress relieving at the same time. Since scandium has already been identified as a critical raw material by European Commission, alternate grain refiners should be explored.
- The as-is printing of existing conventional wrought aluminum alloy grades with comparable mechanical properties is still challenging. However, recent progress has resulted in defect-free printing of *ex situ* reinforced wrought Al-2024 alloy with good mechanical properties, which suggests a possibility of utilizing this strategy for other aluminum alloys.
- Grain refinement through the addition of grain refiners (elements, ceramic particulates) reduces the cracking susceptibility and may also enable the material to withstand higher temperatures.
- *In situ* reinforcement approach for Al-matrix composites can achieve better dispersion and may prove more advantages than *ex situ* reinforcements. Further exploratory work is needed in this direction.

## Acknowledgements

This research was funded by FEDER through programs P2020|COMPETE - Projetos em Copromoção (POCI-01-0247-FEDER-039796\_LISBOA-01-0247-FEDER-039796) and P2020|COMPETE - Programas Mobilizadores (POCI-01-0247-FEDER-046100).

IntechOpen

### **Author details**

Fahad Zafar<sup>1,2\*</sup>, Ana Reis<sup>1,2</sup>, Manuel Vieira<sup>1,2</sup> and Omid Emadinia<sup>2</sup>


1 Faculty of Engineering, University of Porto, Porto, Portugal

2 LAETA/INEGI–Institute of Science and Innovation in Mechanical and Industrial Engineering, Porto, Portugal

\*Address all correspondence to: up202103288@edu.fe.up.pt

### **IntechOpen**

---

© 2023 The Author(s). Licensee IntechOpen. This chapter is distributed under the terms of the Creative Commons Attribution License (<http://creativecommons.org/licenses/by/3.0>), which permits unrestricted use, distribution, and reproduction in any medium, provided the original work is properly cited. 

## References

- [1] Kusoglu IM, Gökce B, Barcikowski S. Research trends in laser powder bed fusion of Al alloys within the last decade. *Additive Manufacturing*. 2020;**36**: 101489. DOI: 10.1016/j.addma.2020.101489
- [2] Olakanmi EO, Cochrane RF, Dalgarno KW. A review on selective laser sintering/melting (SLS/SLM) of aluminium alloy powders: Processing, microstructure, and properties. *Progress in Materials Science*. 2015;**74**:401-477. DOI: 10.1016/j.pmatsci.2015.03.002
- [3] Kenevisi MS, Yu Y, Lin F. A review on additive manufacturing of Al–Cu (2xxx) aluminium alloys, processes and defects. *Materials Science and Technology*. 2021;**37**(9):805-829. DOI: 10.1080/02670836.2021.1958487
- [4] Rometsch PA, Zhu Y, Wu X, Huang A. Review of high-strength aluminium alloys for additive manufacturing by laser powder bed fusion. *Materials and Design*. 2022;**219**: 110779. DOI: 10.1016/j.matdes.2022.110779
- [5] Svetlizky D, Zheng B, Vyatskikh A, Das M, Bose S, Bandyopadhyay A, et al. Laser-based directed energy deposition (DED-LB) of advanced materials. *Materials Science and Engineering A*. 2022;**840**:142967. DOI: 10.1016/j.msea.2022.142967
- [6] Vimal KEK, Naveen Srinivas M, Rajak S. Wire arc additive manufacturing of aluminium alloys: A review. *Materials Today: Proceedings*. 2021;**41**:1139-1145. DOI: 10.1016/j.matpr.2020.09.153
- [7] Kaufmann N, Imran M, Wischeropp TM, Emmelmann C, Siddique S, Walther F. Influence of process parameters on the quality of aluminium alloy EN AW 7075 using selective laser melting (SLM). *Physics Procedia*. 2016;**83**:918-926. DOI: 10.1016/j.phpro.2016.08.096
- [8] Karg MCH, Ahuja B, Wiesenmayer S, Kuryntsev SV, Schmidt M. Effects of process conditions on the mechanical behavior of aluminium wrought alloy EN AW-2219 (AlCu6Mn) additively manufactured by laser beam melting in powder bed. *Micromachines*. 2017;**8**(1): 23. DOI: 10.3390/mi8010023
- [9] Elambasseril J, Benoit MJ, Zhu S, Easton MA, Lui E, Brice CA, et al. Effect of process parameters and grain refinement on hot tearing susceptibility of high strength aluminum alloy 2139 in laser powder bed fusion. *Progress in Additive Manufacturing*. 2022;**2022**:1-15. DOI: 10.1007/s40964-021-00259-2
- [10] Hyer H, Zhou L, Park S, Huynh T, Mehta A, Thapliyal S, et al. Elimination of extraordinarily high cracking susceptibility of aluminum alloy fabricated by laser powder bed fusion. *Journal of Materials Science and Technology*. 2022;**103**:50-58. DOI: 10.1016/j.jmst.2021.06.023
- [11] Zhang H, Zhu H, Qi T, Hu Z, Zeng X. Selective laser melting of high strength Al–Cu–Mg alloys: Processing, microstructure and mechanical properties. *Materials Science and Engineering A*. 2016;**656**:47-54. DOI: 10.1016/j.msea.2015.12.101
- [12] Stopyra W, Gruber K, Smolina I, Kurzynowski T, Kuźnicka B. Laser powder bed fusion of AA7075 alloy: Influence of process parameters on porosity and hot cracking. *Additive Manufacturing*. 2020;**35**:101270. DOI: 10.1016/j.addma.2020.101270



- [13] Aboulkhair NT, Simonelli M, Parry L, Ashcroft I, Tuck C, Hague R. 3D printing of aluminium alloys: Additive manufacturing of aluminium alloys using selective laser melting. *Progress in Materials Science*. 2019;**106**:100578. DOI: 10.1016/j.pmatsci.2019.100578
- [14] Thapliyal S, Komarasamy M, Shukla S, Zhou L, Hyer H, Park S, et al. An integrated computational materials engineering-anchored closed-loop method for design of aluminum alloys for additive manufacturing. *Materialia*. 2020;**9**:100574. DOI: 10.1016/j.mta.2019.100574
- [15] Thapliyal S, Agrawal P, Agrawal P, Nene SS, Mishra RS, McWilliams BA, et al. Segregation engineering of grain boundaries of a metastable Fe-Mn-Co-Cr-Si high entropy alloy with laser-powder bed fusion additive manufacturing. *Acta Materialia*. 2021; **219**:117271 .DOI: 10.1016/j.actamat.2021.117271
- [16] Böhm C, Werz M, Weihe S. Practical approach to eliminate solidification cracks by supplementing AlMg4.5Mn0.7 with AlSi10Mg powder in laser powder bed fusion. *Materials*. 2022;**15**(2):572. DOI: 10.3390/ma15020572
- [17] Zhang X, Zheng H, Yu W. A review on solidification cracks in high-strength aluminum alloys via laser powder bed fusion. *Materials Today: Proceedings*. 2022. DOI: 10.1016/j.matpr.2022.09.366
- [18] Liu S, Guo H. Balling behavior of selective laser melting (SLM) magnesium alloy. *Materials*. 2020; **13**(16):3632
- [19] Altıparmak SC, Yardley VA, Shi Z, Lin J. Challenges in additive manufacturing of high-strength aluminium alloys and current developments in hybrid additive manufacturing. *International Journal of Lightweight Materials and Manufacture*. 2021;**4**(2):246-261. DOI: 10.1016/j.ijlmm.2020.12.004
- [20] Rometsch P, Jia Q, Yang K, Wu X. 14 - Aluminum alloys for selective laser melting—towards improved performance. In: Froes F, Boyer R, editors. *Additive Manufacturing for the Aerospace Industry*. Amsterdam, Netherlands: Elsevier; 2019. pp. 301-325
- [21] Yang KV, Rometsch P, Jarvis T, Rao J, Cao S, Davies C, et al. Porosity formation mechanisms and fatigue response in Al-Si-Mg alloys made by selective laser melting. *Materials Science and Engineering A*. 2018;**712**:166-174. DOI: 10.1016/j.msea.2017.11.078
- [22] Anwar AB, Pham Q-C. Selective laser melting of AlSi10Mg: Effects of scan direction, part placement and inert gas flow velocity on tensile strength. *Journal of Materials Processing Technology*. 2017;**240**:388-396. DOI: 10.1016/j.jmatprotec.2016.10.015
- [23] Wang XJ, Zhang LC, Fang MH, Sercombe TB. The effect of atmosphere on the structure and properties of a selective laser melted Al–12Si alloy. *Materials Science and Engineering A*. 2014;**597**:370-375. DOI: 10.1016/j.msea.2014.01.012
- [24] Kurz W, Fisher DJ. *Fundamentals of Solidification*. Zurich, Switzerland: Trans Tech Publications Limited; 1984. p. 316
- [25] Turnbull D, Vonnegut B. Nucleation catalysis. *Industrial and Engineering Chemistry*. 1952;**44**(6):1292-1298. DOI: 10.1021/ie50510a031
- [26] Zhou L, Pan H, Hyer H, Park S, Bai Y, McWilliams B, et al. Microstructure and tensile property of a novel AlZnMgScZr alloy additively

manufactured by gas atomization and laser powder bed fusion. *Scripta Materialia*. 2019;**158**:24-28

[27] Liu L, Jiang J-T, Cui X-Y, Zhang B, Zhen L, Ringer SP. Correlation between precipitates evolution and mechanical properties of Al-Sc-Zr alloy with Er additions. *Journal of Materials Science and Technology*. 2022;**99**:61-72. DOI: 10.1016/j.jmst.2021.05.031

[28] Roder O, Wirtz T, Gysler A, Lütjering G. Fatigue properties of Al-Mg alloys with and without scandium. *Materials Science and Engineering: A*. 1997;**234–236**:181-184. DOI: 10.1016/S0921-5093(97)00224-4

[29] Horita Z, Furukawa M, Nemoto M, Barnes AJ, Langdon TG. Superplastic forming at high strain rates after severe plastic deformation. *Acta Materialia*. 2000;**48**(14):3633-3640. DOI: 10.1016/S1359-6454(00)00182-8

[30] Palm F, Leuschner R, Schubert T, Kieback B. PM Aluminium and Magnesium 2: Scalmalloy® = A Unique High Strength AlMgSc Type Material Concept Processed by Innovative Technologies for Aerospace Applications. European Congress and Exhibition on Powder Metallurgy European PM Conference Proceedings; 2010: The European Powder Metallurgy Association. 2010

[31] Yang KV, Shi Y, Palm F, Wu X, Rometsch P. Columnar to equiaxed transition in Al-Mg(-Sc)-Zr alloys produced by selective laser melting. *Scripta Materialia*. 2018;**145**:113-117. DOI: 10.1016/j.scriptamat.2017.10.021

[32] Critical raw materials: European Commission. 2020. Available from: [https://single-market-economy.ec.europa.eu/sectors/raw-materials/areas-specific-interest/critical-raw-materials\\_en](https://single-market-economy.ec.europa.eu/sectors/raw-materials/areas-specific-interest/critical-raw-materials_en)

[33] Li X, Li D, Li G, Cai Q. Microstructure, mechanical properties, aging behavior, and corrosion resistance of a laser powder bed fusion fabricated Al-Zn-Mg-Cu-Ta alloy. *Materials Science and Engineering A*. 2022;**832**: 142364. DOI: 10.1016/j.msea.2021.142364

[34] Anderson K, Weritz J, Kaufman JG. 3.3 Heat Treatable Alloys. ASM Handbook, Volume 02A - Aluminum Science and Technology. Ohio, United States of America: ASM International

[35] Aucott L, Huang D, Dong H, Wen S, Marsden J, Rack A, et al. A three-stage mechanistic model for solidification cracking during welding of steel. *Metallurgical and Materials Transactions A*. 2018;**49**(5):1674-1682. DOI: 10.1007/s11661-018-4529-z

[36] Mair P, Goettgens VS, Rainer T, Weinberger N, Letofsky-Papst I, Mitsche S, et al. Laser powder bed fusion of nano-CaB<sub>6</sub> decorated 2024 aluminum alloy. *Journal of Alloys and Compounds*. 2021;**863**:158714. DOI: 10.1016/j.jallcom.2021.158714

[37] Li G, Jadhav SD, Martín A, Montero-Sistiaga ML, Soete J, Sebastian MS, et al. Investigation of solidification and precipitation behavior of Si-Modified 7075 aluminum alloy fabricated by laser-based powder bed fusion. *Metallurgical and Materials Transactions A*. 2021; **52**(1):194-210. DOI: 10.1007/s11661-020-06073-9

[38] Yang F, Wang J, Wen T, Zhang L, Dong X, Qiu D, et al. Developing a novel high-strength Al-Mg-Zn-Si alloy for laser powder bed fusion. *Materials Science and Engineering A*. 2022;**851**:143636. DOI: 10.1016/j.msea.2022.143636

[39] Manca DR, Churyumov AY, Pozdniakov AV, Prosviryakov AS,

Ryabov DK, Krokhin AY, et al. Microstructure and properties of novel heat resistant Al–Ce–Cu alloy for additive manufacturing. *Metals and Materials International*. 2019;**25**(3): 633-640. DOI: 10.1007/s12540-018-00211-0

[40] Pereira JC, Gil E, Solaberrieta L, San Sebastián M, Bilbao Y, Rodríguez PP. Comparison of AlSi7Mg0.6 alloy obtained by selective laser melting and investment casting processes: Microstructure and mechanical properties in as-built/as-cast and heat-treated conditions. *Materials Science and Engineering: A*. 2020;**778**:139124. DOI: 10.1016/j.msea.2020.139124

[41] Ma R, Peng C, Cai Z, Wang R, Zhou Z, Li X, et al. Manipulating the microstructure and tensile properties of selective laser melted Al–Mg–Sc–Zr alloy through heat treatment. *Journal of Alloys and Compounds*. 2020;**831**:154773. DOI: 10.1016/j.jallcom.2020.154773

[42] Li Q, Li G, Lin X, Zhu D, Jiang J, Shi S, et al. Development of a high strength Zr/Sc/Hf-modified Al–Mn–Mg alloy using Laser Powder Bed Fusion: Design of a heterogeneous microstructure incorporating synergistic multiple strengthening mechanisms. *Additive Manufacturing*. 2022;**57**: 102967. DOI: 10.1016/j.addma.2022.102967

[43] Bayoumy D, Kwak K, Boll T, Dietrich S, Schliephake D, Huang J, et al. Origin of non-uniform plasticity in a high-strength Al–Mn–Sc based alloy produced by laser powder bed fusion. *Journal of Materials Science and Technology*. 2022;**103**:121-133. DOI: 10.1016/j.jmst.2021.06.042

[44] Jia Q, Zhang F, Rometsch P, Li J, Mata J, Weyland M, et al. Precipitation kinetics, microstructure evolution and

mechanical behavior of a developed Al–Mn–Sc alloy fabricated by selective laser melting. *Acta Materialia*. 2020;**193**: 239-251. DOI: 10.1016/j.actamat.2020.04.015

[45] Tang H, Geng Y, Bian S, Xu J, Zhang Z. An ultra-high strength over 700 MPa in Al–Mn–Mg–Sc–Zr alloy fabricated by selective laser melting. *Acta Metallurgica Sinica (English Letters)*. 2022;**35**(3):466-474. DOI: 10.1007/s40195-021-01286-2

[46] Bi J, Lei Z, Chen Y, Chen X, Tian Z, Lu N, et al. Microstructure, tensile properties and thermal stability of AlMgSiScZr alloy printed by laser powder bed fusion. *Journal of Materials Science and Technology*. 2021;**69**: 200-211. DOI: 10.1016/j.jmst.2020.08.033

[47] Hu Z, Qi Y, Gao S, Nie X, Zhang H, Zhu H, et al. Aging responses of an Al–Cu alloy fabricated by selective laser melting. *Additive Manufacturing*. 2021;**37**:101635. DOI: 10.1016/j.addma.2020.101635

[48] Nie X, Zhang H, Zhu H, Hu Z, Ke L, Zeng X. Effect of Zr content on formability, microstructure and mechanical properties of selective laser melted Zr modified Al-4.24Cu-1.97Mg-0.56Mn alloys. *Journal of Alloys and Compounds*. 2018;**764**:977-986. DOI: 10.1016/j.jallcom.2018.06.032

[49] Wang Y, Lin X, Kang N, Wang Z, Liu Y, Huang W. Influence of post-heat treatment on the microstructure and mechanical properties of Al–Cu–Mg–Zr alloy manufactured by selective laser melting. *Journal of Materials Science and Technology*. 2022;**111**:35-48. DOI: 10.1016/j.jmst.2021.09.036

[50] Mair P, Kaserer L, Braun J, Stajkovic J, Klein C, Schimbäck D, et al.

Dependence of mechanical properties and microstructure on solidification onset temperature for Al2024–CaB6 alloys processed using laser powder bed fusion. *Materials Science and Engineering A*. 2022;**833**:142552. DOI: 10.1016/j.msea.2021.142552

[51] Qi Y, Zhang H, Nie X, Hu Z, Zhu H, Zeng X. A high strength Al–Li alloy produced by laser powder bed fusion: Densification, microstructure, and mechanical properties. *Additive Manufacturing*. 2020;**35**:101346. DOI: 10.1016/j.addma.2020.101346

[52] Michi RA, Sisco K, Bahl S, Allard LF, Wagner KB, Poplawsky JD, et al. Microstructural evolution and strengthening mechanisms in a heat-treated additively manufactured Al–Cu–Mn–Zr alloy. *Materials Science and Engineering A*. 2022;**840**:142928. DOI: 10.1016/j.msea.2022.142928

[53] Yang KV, Rometsch P, Davies CHJ, Huang A, Wu X. Effect of heat treatment on the microstructure and anisotropy in mechanical properties of A357 alloy produced by selective laser melting. *Materials and Design*. 2018; **154**:275–290. DOI: 10.1016/j.matdes.2018.05.026

[54] Casati R, Coduri M, Riccio M, Rizzi A, Vedani M. Development of a high strength Al–Zn–Si–Mg–Cu alloy for selective laser melting. *Journal of Alloys and Compounds*. 2019;**801**:243–253. DOI: 10.1016/j.jallcom.2019.06.123

[55] Xiao F, Wang S, Wang Y, Shu D, Zhu G, Sun B, et al. Niobium nanoparticle-enabled grain refinement of a crack-free high strength Al–Zn–Mg–Cu alloy manufactured by selective laser melting. *Journal of Alloys and Compounds*. 2022;**900**:163427. DOI: 10.1016/j.jallcom.2021.163427

[56] Huang B, Liu Y, Zhou Z, Cheng W, Liu X. Selective laser melting of 7075 aluminum alloy inoculated by Al–Ti–B: Grain refinement and superior mechanical properties. *Vacuum*. 2022; **200**:111030. DOI: 10.1016/j.vacuum.2022.111030

[57] Li L, Li R, Yuan T, Chen C, Wang M, Yuan J, et al. Microstructures and mechanical properties of Si and Zr modified Al–Zn–Mg–Cu alloy-A comparison between selective laser melting and spark plasma sintering. *Journal of Alloys and Compounds*. 2020; **821**:153520. DOI: 10.1016/j.jallcom.2019.153520

[58] Svetlizky D, Zheng B, Buta T, Zhou Y, Golan O, Breiman U, et al. Directed energy deposition of Al 5xxx alloy using Laser Engineered Net Shaping (LENS®). *Materials and Design*. 2020;**192**:108763. DOI: 10.1016/j.matdes.2020.108763

[59] Wang QZ, Lin X, Kang N, Wen XL, Cao Y, Lu JL, et al. Effect of laser additive manufacturing on the microstructure and mechanical properties of TiB<sub>2</sub> reinforced Al–Cu matrix composite. *Materials Science and Engineering A*. 2022;**840**:142950. DOI: 10.1016/j.msea.2022.142950

[60] Guo C, Singh SC. *Handbook of Laser Technology and Applications: Lasers: Principles and Operations (Volume One)*. Florida, United States of America: CRC Press; 2021

[61] Singh A, Ramakrishnan A, Dinda G. Direct laser metal deposition of Al 7050 alloy. *SAE Technical Paper*; 2017. Report No.: 0148-7191

[62] Zhang J, Song B, Wei Q, Bourell D, Shi Y. A review of selective laser melting of aluminum alloys: Processing, microstructure, property

and developing trends. *Journal of Materials Science and Technology*. 2019; **35**(2):270-284. DOI: 10.1016/j.jmst.2018.09.004

[63] Olakanmi EO. Selective laser sintering/melting (SLS/SLM) of pure Al, Al–Mg, and Al–Si powders: Effect of processing conditions and powder properties. *Journal of Materials Processing Technology*. 2013;**213**(8):1387-1405. DOI: 10.1016/j.jmatprotec.2013.03.009

[64] Ding Y, Muñiz-Lerma JA, Trask M, Chou S, Walker A, Brochu M. Microstructure and mechanical property considerations in additive manufacturing of aluminum alloys. *MRS Bulletin*. 2016;**41**(10):745-751. DOI: 10.1557/mrs.2016.214

[65] Langebeck A, Bohlen A, Rentsch R, Vollertsen F. Mechanical properties of high strength aluminum alloy EN AW-7075 additively manufactured by directed energy deposition. *Meta*. 2020; **10**(5):579. DOI: 10.3390/met10050579

[66] Essien UA, Vaudreuil S. In-situ metal matrix composites development for additive manufacturing: A perspective. *Journal of Achievements in Materials and Manufacturing Engineering*. 2022;**111**(2):78-85. DOI: 10.5604/01.3001.0015.9997

[67] Suryanarayana C. Mechanical alloying and milling. *Progress in Materials Science*. 2001;**46**(1-2):1-184. DOI: 10.1016/S0079-6425(99)00010-9

[68] Yu WH, Sing SL, Chua CK, Kuo CN, Tian XL. Particle-reinforced metal matrix nanocomposites fabricated by selective laser melting: A state of the art review. *Progress in Materials Science*. 2019;**104**:330-379. DOI: 10.1016/j.pmatsci.2019.04.006

[69] Han Q, Setchi R, Evans SL. Synthesis and characterisation of advanced ball-

milled Al-Al<sub>2</sub>O<sub>3</sub> nanocomposites for selective laser melting. *Powder Technology*. 2016;**297**:183-192. DOI: 10.1016/j.powtec.2016.04.015

[70] Yuan P, Gu D. Molten pool behaviour and its physical mechanism during selective laser melting of TiC/AlSi10Mg nanocomposites: Simulation and experiments. *Journal of Physics D: Applied Physics*. 2015;**48**(3):035303. DOI: 10.1088/0022-3727/48/3/035303

[71] Li XP, Ji G, Chen Z, Addad A, Wu Y, Wang H, et al. Selective laser melting of nano-TiB<sub>2</sub> decorated AlSi10Mg alloy with high fracture strength and ductility. *Acta Materialia*. 2017;**129**:183-193. DOI: 10.1016/j.actamat.2017.02.062

[72] Ordonez-Miranda J, Yang R, Alvarado-Gil J. On the thermal conductivity of particulate nanocomposites. *Applied Physics Letters*. 2011;**98**(23):233111. DOI: 10.1063/1.3593387

[73] Sanaty-Zadeh A. Comparison between current models for the strength of particulate-reinforced metal matrix nanocomposites with emphasis on consideration of Hall–Petch effect. *Materials Science and Engineering A*. 2012;**531**:112-118. DOI: 10.1016/j.msea.2011.10.043

[74] Liu X, Liu Y, Zhou Z, Luo W, Zeng Z. Enhanced printability and strength of unweldable AA2024-based nanocomposites fabricated by laser powder bed fusion via nano-TiC-induced grain refinement. *Materials Science and Engineering A*. 2022;**856**:144010. DOI: 10.1016/j.msea.2022.144010

[75] Cheng W, Liu Y, Xiao X, Huang B, Zhou Z, Liu X. Microstructure and mechanical properties of a novel (TiB<sub>2</sub>+TiC)/AlSi10Mg composite prepared by selective laser melting. *Materials Science*

and Engineering A. 2022;**834**:142435.  
DOI: 10.1016/j.msea.2021.142435

[76] Xiao YK, Chen H, Bian ZY, Sun TT, Ding H, Yang Q, et al. Enhancing strength and ductility of AlSi10Mg fabricated by selective laser melting by TiB<sub>2</sub> nanoparticles. *Journal of Materials Science and Technology*. 2022;**109**: 254-266. DOI: 10.1016/j.jmst.2021.08.030

[77] Li S, Cai B, Duan R, Tang L, Song Z, White D, et al. Synchrotron characterisation of ultra-fine grain TiB<sub>2</sub>/Al-Cu composite fabricated by laser powder bed fusion. *Acta Metallurgica Sinica (English Letters)*. 2022;**35**(1):78-92. DOI: 10.1007/s40195-021-01317-y

[78] Ren X, Jiang X, Yuan T, Zhao X, Chen S. Microstructure and properties research of Al-Zn-Mg-Cu alloy with high strength and high elongation fabricated by wire arc additive manufacturing. *Journal of Materials Processing Technology*. 2022;**307**:117665. DOI: 10.1016/j.jmatprotec.2022.117665

[79] Raj Mohan R, Venkatraman R, Raghuraman S. Microstructure and mechanical properties of AlSi10Mg/NbC composite produced by laser-based powder bed fusion (L-PBF) process. *Journal of Metals*. 2022;**75**:155-166. DOI: 10.1007/s11837-022-05428-4